

# Comparison of the glacial isostatic adjustment behaviour in glacially induced fault models

Rebekka Steffen<sup>1</sup>, Holger Steffen<sup>2</sup>, and Patrick Wu<sup>3</sup>

<sup>1</sup>Department of Earth Sciences, Uppsala University, Villavägen 16, 75692 Uppsala, Sweden

<sup>2</sup>Lantmäteriet, Lantmäterigatan 2C, 80182 Gävle, Sweden

<sup>3</sup>Department of Earth Sciences, The University of Hong Kong, Pokfulam Road, Hong Kong

*Correspondence to:* Rebekka Steffen (rebekka.steffen.geo@gmail.com)

**Abstract.** We compare the glacial isostatic adjustment (GIA) behaviour of two approaches developed to model the movement of a glacially induced fault (GIF) as a consequence of stress changes in the Earth's crust caused by the GIA process. GIFs were most likely, but not exclusively reactivated at the end of the last glaciation. Their modelling is complicated as the GIA process involves different spatial and temporal scales and they have to be combined to describe the fault reactivation process accurately. Model approaches have been introduced by Hetzel & Hampel (2005, termed HA in this paper) and Steffen et al. (2014a, termed WU in this paper). These two approaches differ in their geometry, their boundary conditions and the implementation of stress changes. While the WU model is based on GIA models and thus includes the whole mantle down to the core-mantle boundary at a depth of 2891 km, the HA ~~models include~~ model includes only the lithosphere (mostly 100 km) and ~~simulate~~ simulates the mantle using dashpots. ~~They further apply~~ It further applies elastic foundations and a lithostatic pressure at the base of the lithosphere, while the WU ~~models apply~~ model applies elastic foundations at all horizontal boundaries in the model with density contrasts. Using a synthetic ice model as well as the Fennoscandian Ice Sheet, we find large discrepancies in modelled displacement, velocity and stress between these approaches. ~~The~~ Assuming a typical viscosity profile from GIA studies, the HA model has difficulties in explaining relative ~~sea level~~ sea-level curves in Fennoscandia such as the one of Ångermanland (Sweden), ~~where differences of up to 123 m to the data (with data error of 18.7 m) result. The WU model differs by up to 11 m, but falls~~ while the WU model only differs within the error bar of ~~11.6 m~~ the observations. In addition, the HA model cannot predict the typical velocity field pattern in Fennoscandia. As we also find prominent differences in stress, we conclude that the simulation of the mantle using dashpots is not recommended for modelling the GIA process of continental-scale ice sheets. The earth model should consist of both lithosphere and mantle, in order to correctly model the displacement and stress changes during GIA. We emphasize that a thorough modelling of the GIA process is a prerequisite before conclusions on understanding GIF evolution can be drawn.

## 1 Introduction

Geodynamic models are developed to advance our understanding of the many individual as well as overlapping processes of the Earth. A common phenomenon is that several models co-exist for the same process and they should be compared or benchmarked in order to verify that each method works correctly. Benchmark studies thus have been performed for dedicated convection models (e.g. Zhong et al., 2008; Tosi et al., 2015), dynamo models (e.g. Christensen et al., 2001; Jackson et al., 2014) or models of glacial isostatic adjustment (GIA; Spada et al., 2011). The latter describe the response of the Earth in terms of deformation as well as stress, rotation and geopotential changes due to changing ice-ocean load distributions on the Earth's surface. Among other things, the GIA model benchmark showed that the displacement results from models based on the viscoelastic normal mode method are comparable to results from spectral-finite element and finite-element (FE) models, when an earth model is subjected to an ice load. This is of importance as FE models are able to handle faults and lateral heterogeneities in the Earth's subsurface as well as nonlinear or composite rheologies in the mantle.

In this ~~paper~~study, our focus is on the GIA description in glacially induced fault (GIF) models. GIFs represent reactivated faults in or nearby formerly glaciated areas such as North America or northern Europe (e. g. Kujansuu, 1964; Lagerbäck, 1978; Quinlan, 1984; Johnston, 1987; Olesen, 1988; Dyke et al., 1991; Shilts et al., 1992; Fenton, 1994; Arvidsson, 1996; Muir-Wood, 2000; Stewart et al., 2000; Munier & Fenton, 2004; Sauber & Molnia, 2004; Lagerbäck & Sundh, 2008; Brandes et al., 2012). Even historical earthquakes of the last 1200 years in northern Germany are related to the last glaciation of northern Europe (Brandes et al., 2015). Movement of faults under the ice sheets in Laurentia and Fennoscandia was suppressed during glacial loading (Johnston, 1987), but was reactivated near the end of deglaciation (Wu & Hasegawa, 1996).

GIF modelling has been a challenging task as it involves the large spatial scale (> 1000 km) and long time scale ~~tectonics~~tectonic stress (millions of years), the ~~GIA-induced~~GIA-induced stress (thousands of years) and the short-term earthquake motion (a few seconds to minutes) at a fault (of some km length). Nonetheless, two approaches for GIF modelling were introduced in recent years, and both used FE techniques: the first was presented by Hetzel & Hampel (2005, hereafter denoted as HA) based on rather geological aspects and the second by Steffen et al. (2014a) based on the GIA modelling approach by Wu (2004, hereafter WU), which was part of the benchmark study of Spada et al. (2011). Hence, WU has rigorous support from other GIA modelling techniques, while HA has not so far, although it was applied in numerous GIF, but mainly parameter studies (Hampel & Hetzel, 2006; Hampel et al., 2007, 2009; Turpeinen et al., 2009; Hampel et al., 2010a, b). Recently, Steffen et al. (2015) indicated that there are large discrepancies in the vertical deformation behaviour between the two approaches, whose reasons have not been fully investigated yet. Moreover, a comparison of horizontal deformation and stress has not been done as well as a test of the HA approach with a more realistic, continental-scale ice model which has often been

used in GIA investigations. Therefore, our aim in this study is to compare these two approaches in terms of their description of the GIA process to verify (1) ~~if the HA approach is suitable for~~  
65 ~~GIA investigations and~~ the GIA response of both approaches by comparison to a set of typical GIA  
observations, i. e. relative sea-level data and the velocity field, and (2) if GIF results based on ~~the HA~~  
~~approach~~ both approaches are reliable in view of GIF activation due to GIA. A correct description of  
the GIA behaviour is a necessary foundation of GIF models, and is especially important with respect  
to seismic hazard assessments due to GIFs as their response is due to GIA.

70 Before we begin the comparison, it is beneficial to briefly repeat some background knowledge of  
GIA, which occurs due to the lithospheric loading by the ice sheet. The Earth deforms in response to  
this loading: beneath the load the lithosphere moves downward and rebounds once the load is gone.  
During subsidence ~~the mantle flows~~ mantle rocks flow away under the load and ~~moves~~ move  
85 once the ice sheet melts and the lithosphere is rebounding. Due to the ~~viscous~~ viscoelastic behaviour  
of the mantle, the process contains a time-independent elastic component and a time-dependent  
~~viscoelastic~~ viscous component, which delays the achievement of the state of equilibrium. The depth  
of the deformation of the ~~lithosphere and mantle during the~~ GIA process is related to the size of the  
ice sheet and ~~this deformation has its peak value of sensitivity~~ peaks at a depth  $z$  (see Cathles, 1975,  
and Steffen et al., 2015 for a detailed derivation):

$$80 \quad z \simeq \frac{1}{1.7 \sqrt{\frac{1}{L^2} + \frac{1}{M^2}}}, \quad (1)$$

with  $L$  and  $M$  being the characteristic lengths of an elliptical ice sheet. A load size of 2000 km and  
1500 km, for example, which is the north-south and east-west extension of the Fennoscandian Ice  
Sheet (Hughes et al., 2016), respectively, results in a peak value of sensitivity at 706 km depth. How-  
ever, the depth with a half of the peak value gives a conservative estimate of how deep a load size can  
85 "see" into the mantle. The formula is similar to equation 1 except the factor 1.7 is replaced by 0.818,  
which gives a depth of 1467 km. Thus, mantle material at a depth of at least 1500 km is affected due  
to the Fennoscandian Ice Sheet. Any FE model that tries to model GIA-induced displacement and  
stress for comparison with GIA observations (e. g. relative sea-level, GPS or gravity data) needs to  
account for the movement of mantle material at those depths either by using the dedicated boundary  
90 conditions or by extending the model to at least this depth.

The movement of lithosphere and mantle is also accompanied by stress changes. During loading  
(accumulation of ice) vertical and horizontal stresses are induced and during unloading (melting of  
ice) the vertical and horizontal stresses decrease. As soon as the unloading is finished, the vertical  
stresses return to their value before the loading process started. However, as GIA is a viscoelastic  
95 process and stress migrates from the mantle into the lithospheric crust (Wu & Hasegawa, 1996),  
the horizontal stresses return much more slowly to the initial values. The change in stress with  
time is a major ~~parameter for~~ factor in the determination of glacially induced earthquakes as stress  
calculations showed that the reactivation of pre-existing faults was induced by the melting of the ice

sheet (Wu & Hasegawa, 1996; Johnston et al., 1998). Therefore, the stress distribution within GIF  
100 models has to be modelled correctly to allow an accurate analysis of former and current seismic  
hazards induced by glaciation and deglaciation.

Modelling these stress changes is however not straightforward using the FE method. Most FE  
software are ~~based on~~ developed for engineering purposes and only the simple form of the equation  
of motion is solved (Wu, 2004):

$$105 \quad \nabla \cdot \mathbf{S}^{\text{FE}} = 0, \quad (2)$$

with  $\mathbf{S}^{\text{FE}}$  as the stress tensor from FE software. To overcome this problem, Wu (2004) showed that  
the stress obtained from the FE modelling has to be transformed to GIA stresses:

$$\mathbf{S}^{\text{GIA}} = \mathbf{S}^{\text{FE}} + \rho_0 g_0 u_z \mathbf{I}, \quad (3)$$

with  $\mathbf{S}^{\text{GIA}}$  as the GIA stress tensor,  $\rho_0$  and  $g_0$  as the density and gravity for the initial background  
110 state, and  $u_z$  as the vertical component of the displacement vector, to fulfil the simplified GIA equa-  
tion for a flat Earth:

$$\nabla \cdot \mathbf{S}^{\text{GIA}} - \rho_0 g_0 \nabla u_z = 0 \quad (4)$$

(see Wu, 2004, and Steffen et al., 2014a, for a detailed derivation).

In the following, the predicted displacement and stress behaviour from the HA method are com-  
115 pared with those from the WU approach for an earth model without a fault in order to compare the  
GIA contributions only. The next section introduces the two approaches and their two-dimensional  
(2D) model setups. This is followed by a first test in sections 3 and 4, where a synthetic ice model and  
parameters following the study by Hetzel & Hampel (2005) are used. A second test in section 5 will  
show the displacement behaviour of a realistic ice load for both approaches in three dimensions (3D),  
120 using the material parameters and horizontal dimensions of results used in Steffen & Kaufmann  
(2005) and Steffen et al. (2006), but keeping the boundary conditions and vertical dimensions of the  
specific methods.

## 2 Model description

We describe both approaches focusing on the GIA model only and do not include fault geometries.  
125 Additionally, we will describe the synthetic ice model used in the comparison. The FE modelling is  
carried out using the software ABAQUS (Hibbitt et al., 2014).

### 2.1 WU model

The WU model follows the approach developed by Wu (2004). The earth model has a thickness of  
2891 km, from the surface of the Earth to the core-mantle boundary (Fig. 1(a)). Four layers are in-  
130 cluded in the model: the crust, the lithosphere of the mantle, the upper mantle, and the lower mantle.

Each layer is described by density, Young's modulus and Poisson's ratio. Viscosity is applied to the lithospheric, upper and lower mantle only (for values see Fig. 1). At each boundary with density contrast, foundations are applied, which account for the restoring buoyancy force that drives GIA (see Wu, 2004). The model should have a width of at least 10 times of the ice-sheet size to avoid  
135 boundary effects, and the sides of the models are fixed in the horizontal direction. Quadrilateral plane strain elements are used (CPE4).

Figure 1

## 2.2 HA model

140 The HA model follows the approach presented in Hetzel & Hampel (2005). We adopt the same model parameters as used in Hampel et al. (2009, see Fig. 1(b)). The earth model is 100 km thick, from the earth surface to the lithosphere-asthenosphere boundary. The upper and lower mantle are not included in the model. Density, Young's modulus and Poisson's ratio are used for the crustal and lithospheric layer. A viscosity of  $1 \cdot 10^{23}$  Pa·s is used for the lithospheric mantle. At the bottom  
145 of the lithosphere, a lithostatic pressure and elastic foundations are applied. In addition, in e. g. Hetzel & Hampel (2005) dashpots were used as well, to represent the mantle viscosity, but were excluded in the 2D model presented in Hampel et al. (2009). Within the synthetic test, dashpots will not be used. However, we will show in section 5 that the inclusion of dashpots has negligible effects on the HA results. Additionally, the model is loaded with geostatic stresses to obtain a background  
150 stress state to simulate the advection of pre-stress. Due to the geostatic loading, the entire model deforms vertically. This deformation is constant in the entire model and can be subtracted from the displacement results of the ice loading process. The width of the model is 3000 km; hence, larger than the models in Hampel et al. (2009). The vertical sides of the model are fixed in horizontal directions. Triangular plane strain elements are used (CPE3; Hampel et al., 2010a).

155 A study by Schotman et al. (2008) compared the displacement between the WU and HA models, i.e. "implementing the viscosity of the asthenosphere by dashpots instead of a finite element layer" (Hampel et al., 2009). A difference of less than 10% was obtained for the "modeled amount of flexure and rebound" (Hampel et al., 2009). However, Hampel et al. (2009) may have misunderstood the model setup and results of Schotman et al. (2008), who actually did not compare the WU and  
160 HA approach, but rather modified the WU approach by substituting the lower mantle with dashpots. This results in several differences. First the dashpots were not used at the bottom of the lithosphere in Schotman et al. (2008), but instead at the bottom of the 670 km boundary. This is in contrast to the dashpots used in HA models, which are always applied ~~on~~at the bottom of the lithosphere and this varies depending on the study between 80 and 120 km. Second, the upper mantle was included in the  
165 study by Schotman et al. (2008), ~~which~~but is not used in HA models. Third, Schotman et al. (2008) applied foundations at each layer with density contrast following Wu (2004) and thus avoided the

implementation of lithostatic pressure and geostatic stresses. Schotman et al. (2008) conclude that they cannot use dashpot elements to replace the lower mantle as it leads to unacceptable errors for several computed parameters such as geoid height perturbation and horizontal velocities. Vertical deformation at the surface differed by up to 10 %, while in 670 km depth the difference is up to 14 %. Note again that this is for substituting the lower mantle only with dashpots and not for the whole mantle as generally done in the HA models as well as for foundations applied at all layers with density contrasts.

### 2.3 Ice model

All models in sections 3 and 4 are loaded with a 200 km wide and 500 m thick ice sheet. Such ice load affects the Earth's subsurface to a depth of approximately 173 km (using equation 1 with a factor of 0.818 instead of 1.7). The amplitude of the ice load increases to its maximum value over 20 ka and decreases to zero in the following 10 ka. The time increment is 500 a. The load is modelled as pressure in the software ABAQUS (Hibbitt et al., 2014). [In section 5, a realistic ice model is used.](#)

## 3 Comparison of the displacement

The vertical displacement is obtained for both model approaches and only the geostatic displacement in the HA model is subtracted (0.64 m) from the FE modelling results. Fig. 2 shows the vertical displacement at three different locations at the surface of the model: at the centre of the model (0 km), at the ice margin (100 km) and 400 km away from the margin (500 km). Results at selected time steps are also listed in Table 1.

Figure 2

Table 1

The HA model shows a gradual subsiding of the crust beneath the ice sheet during loading to -78.1 m at 0 km and -62.9 m at 100 km (Fig. 2). This is followed by an instantaneous elastic response as soon as deloading starts. At 30 ka (end of deloading) the vertical displacement is only -2.5 m at 0 km and -1.3 m at 100 km, and the uplift rate changes from 7.6 m/ka to 0.02 m/ka at the centre. At a location outside of the ice sheet, the vertical displacement increases up to 2.1 m and decreases with the start of deloading to the end of deloading to 0.4 m.

The vertical displacement obtained from model WU is smaller beneath the ice sheet (Fig. 2), but larger at the third location (500 km). During loading, the crust subsides to -53.0 m at 0 km and -40.9 m at 100 km. The subsidence is not linear during loading due to the viscoelasticity of the man-

tle. Maximum displacement is also not directly at maximum glaciation, but within this example 1 ka later. The deloading process is accompanied by a slow uplift of the crust. The vertical displacement increases to -19.4 m and -15.7 m at 0 km and 100 km, respectively, at the end of deglaciation. After deloading, the uplift is still ongoing and the uplift velocity changes from 5.3 m/ka to 3.6 m/ka. At 205 500 km, the vertical displacement increases during loading to 4.7 m and decreases during and after deloading back to 0 m, indicating that this location is within the peripheral bulge. The subsiding of the crust at this location is not instantaneous, and a delay of 2 ka is observed.

The vertical displacement shows large differences (25.7 m at maximum glaciation) between the models HA and WU. Whereas the WU model shows a viscoelastic response of the earth model to the 210 loading and unloading of the ice model, the HA model shows almost exclusively an elastic response. We refer this difference to the different model dimensions in depth and thus the missing mantle layers. An ice load of 200 km width, has its peak value in sensitivity at a depth of 83 km, half of the peak value is reached at a depth of 173 km and a quarter still at 223 km. The model depth of only 100 km depth can therefore not be recommended when displacement changes due to the viscoelastic 215 nature of the GIA process are calculated. This naturally alters the stress distribution and its change (stress migration), which we will investigate next.

## 4 Comparison of the stress

The horizontal stresses of the HA and WU models are shown in Fig. 3. Stresses from the WU model were transformed according to the equations described above. However, the stresses from 220 HA models are not changed as the unmodified stresses ( $S^{FE}$ ) are used by Hetzel & Hampel (2005) within the fault modelling steps. In contrast, Steffen et al. (2014a) use the modified stresses ( $S^{GIA}$ ) for their fault modelling. The vertical stresses of both approaches are almost identical (see Table 1) as this stress is induced by the load only.

### 4.1 Horizontal stress

225 The horizontal stress is a function of the size of the ice model, the earth model parameters, and the viscous behaviour of the mantle due to the stress migration from mantle to lithosphere. For a comparison of the horizontal stress results, the change with depth for two different time points is shown for both models (Fig. 3). The first time point is at maximum glaciation (20 ka, Fig. 3(a), (b)). The general distribution of the horizontal stress at glacial maximum is similar between WU and HA; however, 230 the stress magnitude differs between both methods. While HA models reach an amplitude of almost -10.3 MPa below the ice sheet within the crust, models by WU show only values of -8.4 MPa. At the bottom of the lithosphere (at 100 km), larger stress magnitudes are also obtained for HA models (13.8 MPa) compared to WU (10.8 MPa). The second time point used in the comparison shows larger differences within the stress magnitudes and the general distribution (Fig. 3(c), (d)). This time point

235 corresponds with the end of deglaciation, and therefore reflects the time, when most known GIFs  
got reactivated. While models by HA show only a stress magnitude of -0.2 MPa below the ice sheet  
at a depth of 5 km (Table 1), WU models reach -2.1 MPa. A difference of 1.9 MPa is able to change  
the potential of a GIF from active to inactive or vice versa as well as the magnitude of the earthquake.

240 Figure 3

#### 4.2 Differential stress

The differential stress is of high importance in stress field analyses. Models by HA show an in-  
stantaneous increase in 5 km depth in the stress magnitude during glaciation and an instantaneous  
decrease during deglaciation (Fig. 4). At the end of deglaciation, the rate of the stress magnitude  
245 changes significantly. The behaviour of the stress magnitude curve is similar to the curve of the ver-  
tical displacement by HA, dominated by the elastic behaviour of the model. In contrast, the models  
by WU show a viscoelastic behaviour, similar to the vertical displacement of WU (Fig. 4). At the end  
of deglaciation, the differential stresses are larger at all locations, which would favour a reactivation  
of a GIF at those time points.

250

Figure 4

### 5 Comparison for a realistic ice sheet

The results obtained above indicate that the modelling approach from Hetzel & Hampel (2005) is  
not able to ~~capture the~~ describe the typical GIA response of displacement and horizontal stresses ac-  
255 curately using a synthetic ice sheet. A comparison of their modelling approach to observed datasets  
(e.g. relative ~~sea level~~ sea-level, GPS or gravity data) has not been demonstrated so far. As such com-  
parison is an important tool to properly validate the modelling approach, the results of a model based  
on the modelling approach by Wu (2004) and Hetzel & Hampel (2005) are compared to relative ~~sea~~  
level sea-level (RSL) data as well as observed Global Navigation Satellite System (GNSS) velocities  
260 using a 3D flat-earth model with realistic ice history.

The WU model has again a thickness of 2891 km using four layers (crust, lithospheric mantle,  
upper mantle, lower mantle) and a model width of 130,000 km is used to avoid boundary effects  
(Steffen et al., 2006). The HA model has a thickness of 120 km, which is a typical lithospheric  
thickness estimated from observations for Fennoscandia (Steffen & Kaufmann, 2005; Steffen & Wu,  
265 2011) and used in the WU model as well. The width of the HA model is the same as for the WU  
model. Both models are meshed using brick elements (C3D8). We tested two different subsets of  
the model, one without dashpots at the base of the model (thus base of the lithosphere) and one  
with dashpots, to show the effect of dashpots used in HA models. The dashpot-property value is set

equal to the upper-mantle viscosity used in the WU model ( $4 \cdot 10^{20}$  Pa·s) and is unlike that used in  
270 HA models where the viscosities are too low to be representative of the whole mantle (Steffen et al.,  
2015). [A lower mantle viscosity of  \$1 \cdot 10^{22}\$  Pa·s is used in the WU model \(Fig. 1\)](#). The Fennoscandian  
ice sheet model RSES by Lambeck et al. (1998) is used.

Two RSL curves are chosen based on their location. The first set of RSL data is from Ångermanland,  
land, which is close to the centre of rebound. The second RSL curve is in the Netherlands, hence,  
275 outside of the Fennoscandian Ice Sheet in the peripheral bulge area. The results show large discrepancies  
between the two modelling approaches. For the HA model the discrepancies between the predictions and the  
observations reach 123 m and 22 m for Ångermanland (Sweden) and Leeuwarden (Netherlands), respectively  
(Fig. 5). In contrast, the results following Wu (2004) match the observations better and the discrepancies  
are much smaller: 11 m and 5.2 m for Ångermanland (Sweden)  
280 and Leeuwarden (Netherlands), respectively (Fig. 5).

Figure 5

In addition, we see that the HA models with and without dashpots show no difference. Hence,  
285 there is no effect of the dashpots and thus of the viscoelasticity of the underlying mantle. We attribute  
this behaviour to the large foundation applied at the base of the lithosphere, which Hampel et al.  
(2009) calculate taking into account the whole density of the asthenosphere instead of the density  
contrast.

The observed uplift velocity of Fennoscandia reaches its maximum of 10 mm/a in the Gulf of  
290 Bothnia (Fig. 6(a)), which is also predicted by the WU model [with this earth model configuration  
known from former GIA studies](#) (Fig. 6(b)). In addition, the modelled horizontal velocity field shows  
in general a similar pattern as the GNSS observations. A perfect match is not possible with flat-  
earth FE models due to the horizontal boundary conditions and partly due to the lack of sphericity  
(Schotman et al., 2008). In contrast, the velocity fields obtained from the models following the ap-  
295 proaches by Hampel et al. (2009) and Hetzel & Hampel (2005) are about zero in the entire region  
(Fig. 6(c), (d)), and thus cannot capture the typical uplift signal. This is due to the very high viscos-  
ity ( $1 \cdot 10^{23}$  Pa·s) in their lithospheric mantle so that its Maxwell [relaxation](#) time is of the order of  
100 ka, thus it behaves almost exclusively elastically during the glacial cycle. Even if the dashpots  
are present, they cannot fully represent the viscoelastic relaxation of the mantle and the upward mi-  
300 gration of stress, which is a result of the high foundation applied at the base of the model.

Figure 6

[To verify this observation, other viscosities were applied at the dashpots in the HA model and  
305 in the upper mantle of the WU model. An upper mantle viscosity of  \$4 \cdot 10^{18}\$  Pa·s is used in a first](#)

test. This low value implies a shorter Maxwell relaxation time, which leads to a rapid rebound of the lithosphere. The lithosphere shows an almost instantaneous reaction to changes in the ice load. This is visible for the WU and HA models in Fig. 7; however, nothing has changed for the HA model when compared to results using a viscosity of  $4 \cdot 10^{20}$  Pa·s for the dashpots. In a second test, a higher viscosity of  $4 \cdot 10^{22}$  Pa·s is used for the dashpots in the HA model as well as upper mantle viscosity in the WU model. If the material has a high viscosity, the Maxwell relaxation time is also increased. This implies that the mantle is too stiff and prevents sinking of the lithosphere into the mantle. Only for longer time than the Maxwell relaxation time the mantle will behave viscoelastically and deform. This results in a small deformation during loading and hence, a small amount of land uplift during and after deglaciation. While the WU model shows exactly this behaviour in Fig. 8, the HA model shows no variation in Figs. 5 and 7 due to viscosity variations for the dashpot. This implies that any viscosity could be used for the dashpot, as the foundation value is set too high, and the dashpots cannot be used to model the GIA process.

320 [Figure 7](#)

[Figure 8](#)

## 6 Conclusions

325 The GIA process plays an important role in the reactivation of pre-existing faults (GIFs). Hence, the modelling of GIFs must be based on the correct description of the GIA process in the models. Two different GIF modelling approaches, one based on Steffen et al. (2014a) and Wu (2004), and the other based on Hetzel & Hampel (2005), were compared for their displacement and stress behaviour due to GIA during a loading process neglecting the effect of a fault. In our first test, a synthetic ice sheet was applied. Differences in the vertical displacement of up to 25.7 m (49 %) and in the differential stress magnitudes of up to 1.9 MPa (90 %) were obtained between the approaches. The general behaviour of the models presented in the displacement curve shows also large discrepancies, as the model following Hetzel & Hampel (2005) indicates almost exclusively an elastic response to the ice load, whereas the model following Wu (2004) reveals its viscoelastic response [generally known from](#)  
335 [former GIA studies](#). It should be noted that some slight viscoelastic behaviour in the deformation and stress changes from HA models is solely due to the viscoelastic lithosphere and not the mantle. Previous studies with HA models (Turpeinen et al., 2009; Hampel et al., 2009) showed viscoelastic displacements using low viscosity values of  $4 \cdot 10^{18}$  Pa·s for the lithosphere and  $1 \cdot 10^{19}$  Pa·s for the lower crust, which give Maxwell [relaxation](#) times of the order of ten years. Thus they relax too fast  
340 and too early to be of importance to the triggering of GIF movement by the GIA process.

Applying a realistic ice sheet and using the same vertical dimensions of each modelling approach presents a good fit to RSL and GPS observations for the model after Wu (2004), but leaves large differences in the model of Hetzel & Hampel (2005). The uplift velocities predicted by their approach exhibit no significant uplift today in entire northern Europe due to the last glaciation. As the method  
345 after Wu (2004) was recently benchmarked to GIA models using the commonly used viscoelastic normal-mode method (Schotman et al., 2008; Spada et al., 2011) and performing excellently there, we suggest that this approach is preferable when simulating GIFs, i. e. if continental-scale ice sheets are taken into account. Parameter tests for GIF with this method can be found in Steffen et al. (2014b, c). However, both approaches are also limited with respect to other parameters, as temperature  
350 dependence, change in elastic thickness of the lithosphere during loading, convection in the mantle as well as realistic density structures are not included, which might effect the displacement and stress changes induced by GIA. Nevertheless, the importance of the mantle is shown here, which is a major parameter in GIA models.

Unfortunately, the approach by Hetzel & Hampel (2005) cannot be recommended ~~due to their~~  
355 ~~poor performance for GIF studies due to the results~~ in GIA investigations obtained within this study, which are a major prerequisite for GIF analysis. ~~Moreover, our comparison to GIA observations questions all results of earlier studies applying this approach.~~ The approach by Hetzel & Hampel (2005) may only be feasible if the load (e. g. ice or water) is small enough to reach maximum sensitivity in the lithosphere. Steffen et al. (2015) showed that this is possible for load dimensions of  
360 <100 km diameter; however, all studies to date applying the HA approach used partly much larger loads, and hence these results have to be treated with care..

### Code availability

The input files of the HA and WU model using a synthetic ice sheet are included in the supplementary material (HA.inp and WU.inp). The set-up of the HA model is obtained from Hampel et al.  
365 (2009, 2010a). The input files of the 3D models using a realistic ice sheet are available upon request, however, the structure of the input files is the same as for the HA.inp and WU.inp.

*Acknowledgements.* We are very grateful for the excellent reviews and numerous valuable suggestions from two anonymous referees and the Editor, Philippe Huybrechts, which have greatly improved this manuscript. We would like to thank Björn Lund and Peter Schmidt (Uppsala University) for several discussions about the  
370 modelling approaches as well as Hugo Schotman for details on the models used in Schotman et al. (2008).

## References

- Arvidsson, R. (1996): Fennoscandian Earthquakes: Whole Crustal Rupturing Related to Postglacial Rebound, *Science*, **274**, 744-746, doi:10.1126/science.274.5288.744.
- Brandes, C., Winsemann, J., Roskosch, J., Meinsen, J., Tanner, D.C., Tsukamoto, S., Frechen, M., Steffen, H.,  
375 Wu, P. (2012): Activity along the Osning Thrust in Central Europe during the late Weichselian: ice-sheet and  
lithosphere interactions, *Quat. Sci. Rev.*, **38**, 49-62, doi:10.1016/j.quascirev.2012.01.021.
- Brandes, C., Steffen, H., Steffen, R., Wu, P. (2015): Intraplate seismicity in northern Central Europe is induced  
by the last glaciation, *Geology*, **43**(7), 611-614, doi:10.1130/G36710.1.
- Cathles, L.M. (1975): The viscosity of the earth's mantle, *Princeton University Press, Princeton, USA*.
- 380 Christensen, U.R., Aubert, J., Cardin, P., Dormy, E., Gibbons, S., Glatzmaier, G.A., Grote, E., Honkura, Y.,  
Jones, C., Kono, M., Matsushima, M., Sakuraba, A., Takahashi, F., Tilgner, A., Wicht, J., Zhang, K. (2001):  
A numerical dynamo benchmark, *Phys. Earth planet. Inter.*, **128**, 25-34, doi:10.1016/S0031-9201(01)00275-  
8.
- Dyke, A.S., Morris, T.F., Green, D.E.C. (1991): Postglacial tectonic and sea level history of the central Canadian  
385 Arctic, *Geol. Survey Canada Bull.*, **397**.
- Fenton, C. (1994): Postglacial faulting in Eastern Canada, *Geol. Survey Canada Open File*, **2774**, 94 pp..
- Hampel, A., Hetzel, R. (2006): Response of normal faults to glacial-interglacial fluctuations of ice and water  
masses on Earth's surface, *J. Geophys. Res.*, **111**, B06406, doi:10.1029/2005JB004124.
- Hampel, A., Hetzel, R., Densmore, A.L. (2007): Postglacial slip-rate increase on the Teton normal fault, north-  
390 ern Basin and Range Province, caused by melting of the Yellowstone ice cap and deglaciation of the Teton  
Range?, *Geology*, **35**, 1107-1110, doi:10.1130/G24093A.1.
- Hampel, A., Hetzel, R., Maniatis, G., Karow, T. (2009): Three-dimensional numerical modeling of slip rate vari-  
ations on normal and thrust fault arrays during ice cap growth and melting, *J. Geophys. Res.*, **114**, B08406,  
doi:10.1029/2008JB006113.
- 395 Hampel, A., Karow, T., Maniatis, G., Hetzel, R. (2010a): Slip rate variations on faults during glacial loading and  
post-glacial unloading: implications for the viscosity structure of the lithosphere, *J. Geolog. Soc., London*,  
**167**, 385-399, doi:10.1144/0016-76492008-137.
- Hampel, A., Hetzel, R., Maniatis, G. (2010b): Response of faults to climate-driven changes in ice and water  
volumes on Earth's surface, *Phil. Trans. R. Soc. A*, **368**, 2501-2517, doi:10.1098/rsta.2010.0031.
- 400 Hetzel, R., Hampel, A. (2005): Slip rate variations on normal faults during glacial-interglacial changes in surface  
loads, *Nature*, **435**, 81-84, doi:10.1038/nature03562.
- Hibbitt, D., Karlsson, B., Sorensen, P. (2014): Getting Started with ABAQUS - Version (6.14), Hibbitt, Karlsson  
& Sorensen, Inc.
- Hughes, A.L.C., Gyllencreutz, R., Lohne, Ø.S., Mangerud, J., Svendsen, J. I. (2016): The last Eurasian  
405 ice sheets - a chronological database and time-slice reconstruction, DATED-1, *Boreas*, **45**, 1-45,  
doi:10.1111/bor.12142.
- Jackson, A., Sheyko, A., Marti, P., Tilgner, A., Cébron, D., Vantieghema, S., Simitev, R., Busse, F., Zhan, X.,  
Schubert, G., Takehiro, S., Sasaki, Y., Hayashi, Y.-Y., Ribeiro, A., Nore, C., Guermond, J.-L. (2014): A  
spherical shell numerical dynamo benchmark with pseudo vacuum magnetic boundary conditions, *Geophys.*  
410 *J. Int.*, **196**(2), 712-723, doi:10.1093/gji/ggt425.

- Johnston, A.C. (1987): Suppression of earthquakes by large continental ice sheets, *Nature*, **330**, 467-469, doi:10.1038/330467a0.
- Johnston, P., Wu, P., Lambeck, K. (1998): Dependence of horizontal stress magnitude on load dimension in glacial rebound models, *Geophys. J. Int.*, **132**, 41-60, doi:10.1046/j.1365-246x.1998.00387.x.
- 415 Kierulf, H.P., Steffen, H., Simpson, M.J.R., Lidberg, M., Wu, P., Wang, H. (2014): A GPS velocity field for Fennoscandia and a consistent comparison to glacial isostatic adjustment models, *J. Geophys. Res.*, **119**, 6613-6629, doi:10.1002/2013JB010889.
- Kujansuu, R. (1964): Nuorista siirroksista Lappissa. Summary: Recent faults in Lapland, *Geologi*, **16**, 30-36.
- Lagerbäck, R. (1978): Neotectonic structures in northern Sweden, *Geologiska Föreningen i Stockholm Förhandlingar*, **100**, 263-269, doi:10.1080/11035897809452533.
- 420 Lagerbäck, R., Sundh, M. (2008): Early Holocene faulting and paleoseismicity in northern Sweden, *Sveriges geologiska undersökning - Research paper*, **836**.
- Lambeck K., Smither, C., Johnston, P. (1998): Sea-level change, glacial rebound and mantle viscosity for northern Europe, *Geophys. J. Int.*, **134**, 102-144, doi:10.1046/j.1365-246x.1998.00541.x.
- 425 Muir-Wood, R. (2000): Deglaciation Seismotectonics: a principal influence on intraplate seismogenesis at high latitudes, *Quat. Sci. Rev.*, **19**, 1399-1411, doi:10.1016/S0277-3791(00)00069-X.
- Munier, R., Fenton, C. (2004): Review of postglacial faulting - Current understanding and directions for future studies, In: *Respect distances - Rationale and means of computation*, Swedish Nuclear Fuel and Waste Management Co., Stockholm, Report R-04-17, 62 pp..
- 430 Olesen, O. (1988): The Stuoragurra Fault, evidence of neotectonics in the Precambrian of Finnmark, northern Norway, *Norsk Geologisk Tidsskrift*, **68**, 107-118.
- Quinlan, G. (1984): Postglacial rebound and the focal mechanisms of eastern Canadian earthquakes, *Can. J. Earth Sci.*, **21**, 1018-1023, doi:10.1139/e84-106.
- Sauber, J., Molnia, B. (2004): Glacier ice mass fluctuations and fault instability in tectonically active southern 435 Alaska, *Glob. Planet. Change*, **42**, 279-293, doi:10.1016/j.gloplacha.2003.11.012.
- Schotman, H.H.A., Wu, P., Vermeersen, L.L.A. (2008): Regional perturbations in a global background model of glacial isostasy, *Phys. Earth Planet. In.*, **171**, 323-335, doi:10.1016/j.pepi.2008.02.010.
- Shilts, W.W., Rappol, M., Blais, A. (1992): Evidence of late and postglacial seismic activity in the Témiscouata-Madawaska Valley, Quebec - New Brunswick, Canada, *Can. J. Earth Sci.*, **29**, 1043-1059, doi:10.1139/e92-440 085.
- Spada, G., Barletta, V.R., Klemann, V., Riva, R.E.M., Martinec, Z., Gasperini, P., Lund, B., Wolf, D., Vermeersen, L.L.A., King, M.A. (2011): A benchmark study for glacial isostatic adjustment codes, *Geophys. J. Int.*, **185**, 106-132, doi:10.1111/j.1365-246X.2011.04952.x.
- Steffen, H., Kaufmann, G. (2005): Glacial isostatic adjustment of Scandinavia and northwestern Europe and 445 the radial viscosity structure of the Earth's mantle, *Geophys. J. Int.*, **163**, 801-812, doi:10.1111/j.1365-246X.2005.02740.x.
- Steffen, H., Wu, P. (2011): Glacial isostatic adjustment in Fennoscandia - A review of data and modeling, *J. Geodyn.*, **52**, 169-204, doi:10.1016/j.jog.2011.03.002.
- Steffen H., Kaufmann, G., Wu, P. (2006): Three-dimensional finite-element modelling of the glacial isostatic 450 adjustment in Fennoscandia, *Earth Planet. Sci. Lett.*, **250**, 358-375, doi:10.1016/j.epsl.2006.08.003.

- Steffen, R., Eaton, D.W., Wu, P. (2012): Moment tensors, state of stress and their relation to post-glacial rebound in northeastern Canada, *Geophys. J. Int.*, **189**, 1741-1752, doi:10.1111/j.1365-246X.2012.05452.x.
- Steffen, R., Wu, P., Steffen, H., Eaton, D.W. (2014a): On the implementation of faults in finite-element glacial isostatic adjustment models, *Comp. Geosciences*, **62**, 150-159, doi:10.1016/j.cageo.2013.06.012.
- 455 Steffen, R., Wu, P., Steffen, H., Eaton, D.W. (2014b): The effect of earth rheology and ice-sheet size on faultslip and magnitude of postglacial earthquakes, *Earth Planet. Sc. Lett.*, **388**, 71-80, doi:10.1016/j.epsl.2013.11.058.
- Steffen, R., Steffen, H., Wu, P., Eaton, D.W. (2014c): Stress and fault parameters affecting fault slip magnitude and activation time during a glacial cycle, *Tectonics*, **33**(7), 1461-1476, doi:10.1002/2013TC003450.
- 460 Steffen, R., Steffen, H., Wu, P., Eaton, D.W. (2015): Reply to comment by Hampel et al. on "Stress and fault parameters affecting fault slip magnitude and activation time during a glacial cycle", *Tectonics*, **34**(11), 2359-2366, doi:10.1002/2015TC003992.
- Stewart, I.S., Sauber, J., Rose, J. (2000): Glacio-seismotectonics: ice sheets, crustal deformation and seismicity, *Quat. Sci. Rev.*, **19**, 1367-1389, doi:10.1016/S0277-3791(00)00094-9.
- 465 Tosi N., Stein, C., Noack, L., Hüttig, C., Maierová, P., Samuel, H., Davies, R., Wilson, C., Kramer, S., Thieulot, C., Glerum, A., Fraters, M., Spakman, W., Rozel, A., Tackley, P. (2015): A community benchmark for viscoplastic thermal convection in a 2-D square box, *Geochem. Geophys. Geosyst.*, **16**(7), 2175-2196, doi:10.1002/2015GC005807.
- Turpeinen, H., Hampel, A., Karow, T., Maniatis, G. (2009): Effect of ice sheet growth and melting on the slip  
470 evolution of thrust faults, *Earth planet. Sci. Lett.*, **269**, 230-241, doi:10.1016/j.epsl.2008.02.017.
- Wu, P. (2004): Using commercial Finite element packages for the study of earth deformations, sea levels and the state of stress, *Geophys. J. Int.*, **158**, 401-408, doi:10.1111/j.1365-246X.2004.02338.x.
- Wu, P., Hasegawa, H.S. (1996): Induced stresses and fault potential in Eastern Canada due to a disc load: a preliminary analysis, *Geophys. J. Int.*, **125**, 415-430, doi:10.1111/j.1365-246X.1996.tb00008.x.
- 475 Zhong, S., McNamara, A., Tan, E., Moresi, L., Gurnis, M. (2008): A benchmark study on mantle convection in a 3-D spherical shell using CitcomS, *Geochem. Geophys. Geosyst.*, **9**(10), doi:10.1029/2008GC002048.

Captions to Figures:

**Figure 1:**

480 Schematic sketch of the model structures following the approach by Wu (2004, (a)) and by Hetzel & Hampel (2005, (b)) used for the comparison of displacement and stress using a synthetic ice sheet. The width of the model is only changed when using the realistic ice sheet with 130,000 km for both model types. In addition, the lithospheric thickness is increased from 100 km to 120 km, when using a realistic ice sheet model. (b) is adapted from Hetzel & Hampel (2005).

485

**Figure 2:**

Vertical displacement at the surface for the model HA (red) and the model WU (blue). Three different locations are shown: beneath the centre of the ice sheet (0 km, solid line), at the boundary of the ice sheet (100 km, dashed line), and 400 km away from the ice sheet border (500 km, dotted line).

490 The increase and decrease of the load is shown in the upper part of the figure as purple curve.

**Figure 3:**

Horizontal stresses for two time points for model HA (left) and model WU (right). Upper row ((a) and (b)) is for glacial maximum (20 ka) and lower row ((c) and (d)) is for end of deglaciation (30 ka).

495 The size of the ice sheet is shown as purple bar on top of each model.

**Figure 4:**

Differential stress at 5 km depth of the model HA (red) and model WU (blue). Locations as in Fig. 2.

500 **Figure 5:**

Observed and modelled relative sea-level (RSL) curves for (a) Leeuwarden (Netherlands) and (b) Ångermanland (Sweden). Solid lines are modelled predictions using the RSES Fennoscandian Ice Sheet model (Lambeck et al., 1998) for models following the approach by Wu (2004, blue) with a depth of 2891 km, by Hampel et al. (2009, red) with a depth of 120 km and without dashpots at the base of the model, and by Hetzel & Hampel (2005, green) with a depth of 120 km and using dashpots at the base of the model to simulate the viscosity of the upper mantle. [An upper mantle viscosity of  \$4 \cdot 10^{20}\$  Pa·s is sued.](#) The observations from RSL data are shown in black, including the error in time and height.

510 **Figure 6:**

Observed and modelled velocities in northern Europe. (a) Global Navigation Satellite System (GNSS) observations from Kierulf et al. (2014). (b) - (d) Modelled velocities using the RSES Fennoscandian Ice Sheet model (Lambeck et al., 1998) for models following the approach (b) by Wu (2004) with a

depth of 2891 km, (c) by Hampel et al. (2009) with a depth of 120 km and without dashpots at the  
515 base of the model, and (d) by Hetzel & Hampel (2005) with a depth of 120 km and using dashpots  
at the base of the model to simulate the viscosity of the upper mantle.

**Figure 7:**

Same as Fig. 5, but an upper mantle viscosity of  $4 \cdot 10^{18}$  Pa·s is used.

520

**Figure 8:**

Same as Fig. 5, but an upper mantle viscosity of  $4 \cdot 10^{22}$  Pa·s is used.

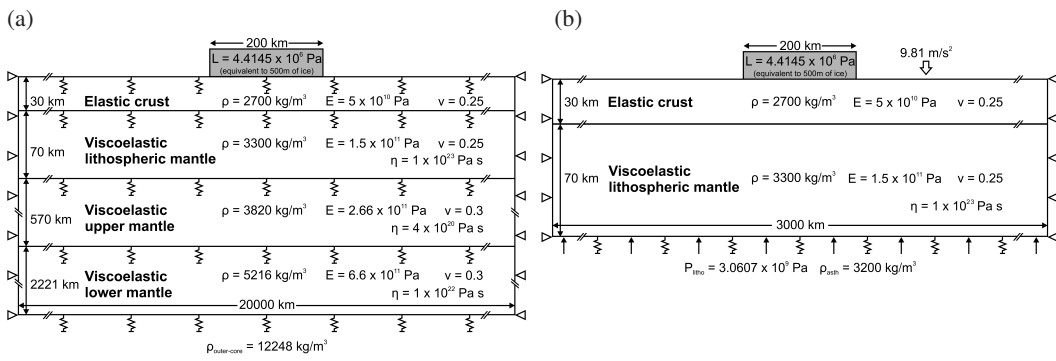


Figure 1.

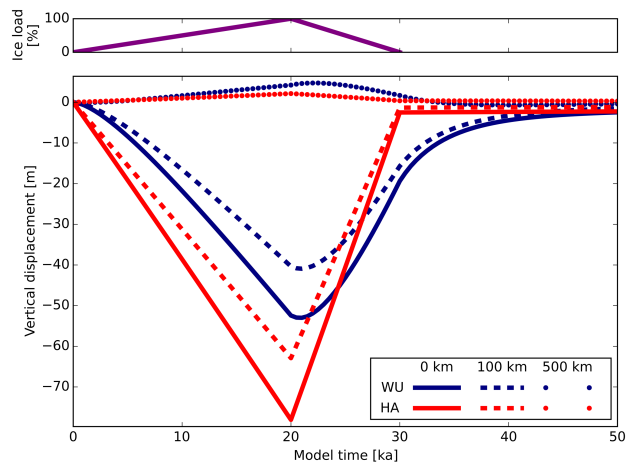


Figure 2.

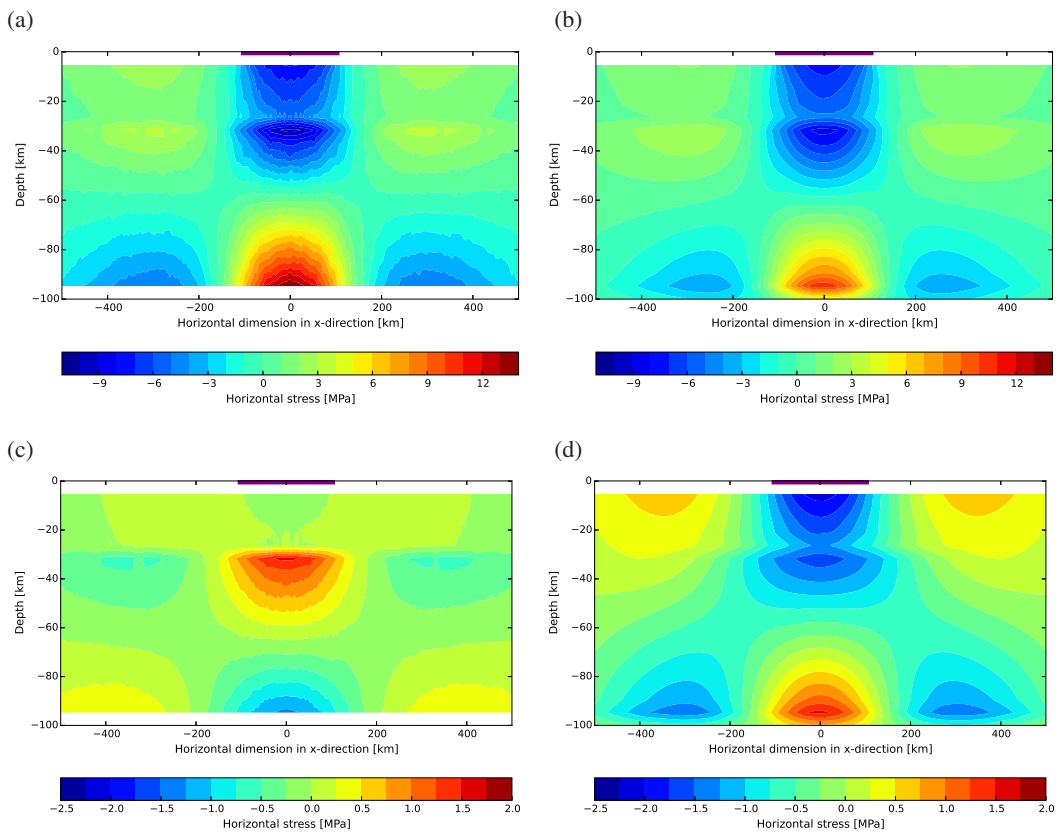


Figure 3.

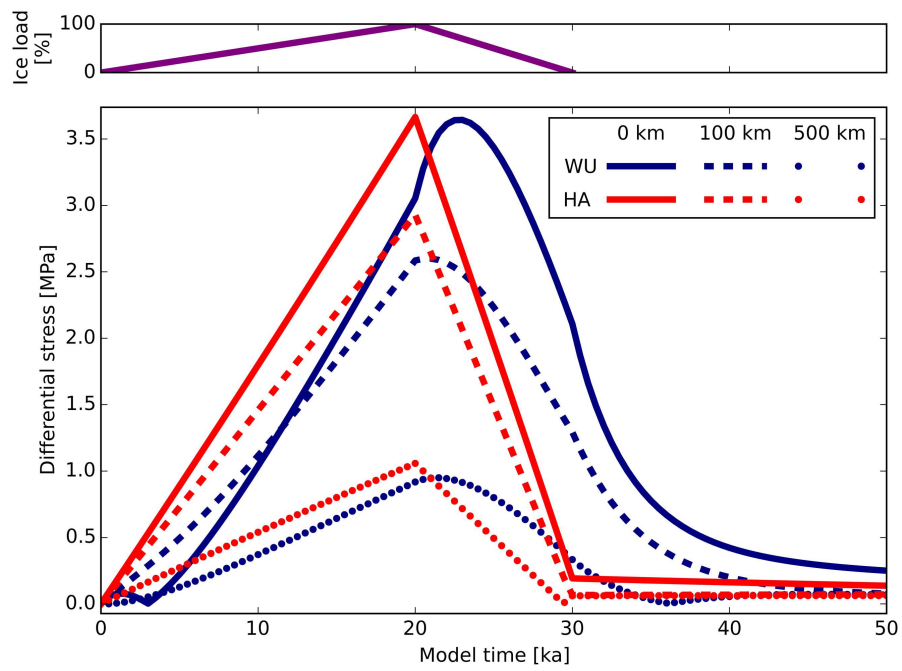


Figure 4.

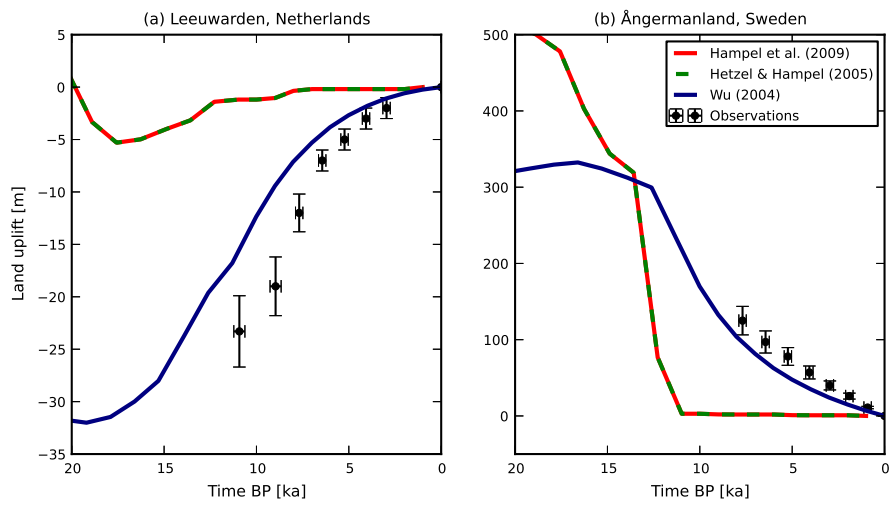


Figure 5.

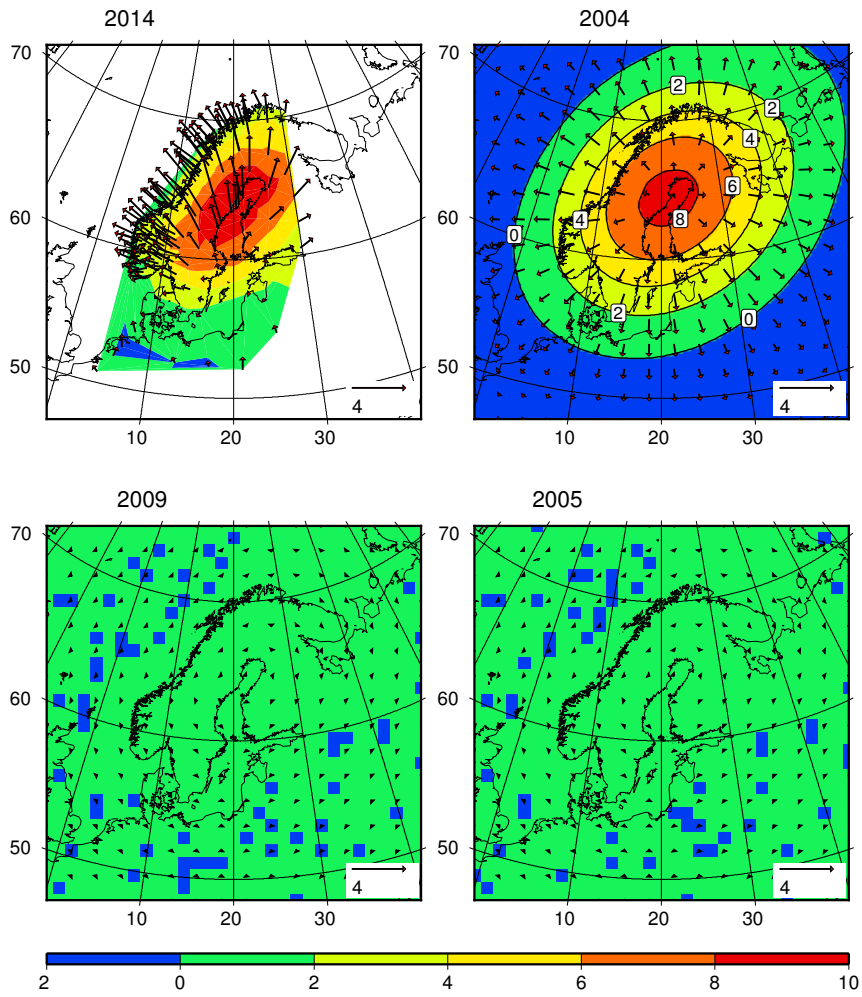


Figure 6.

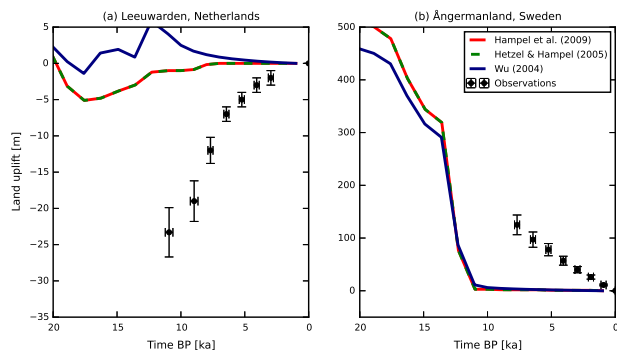


Figure 7.

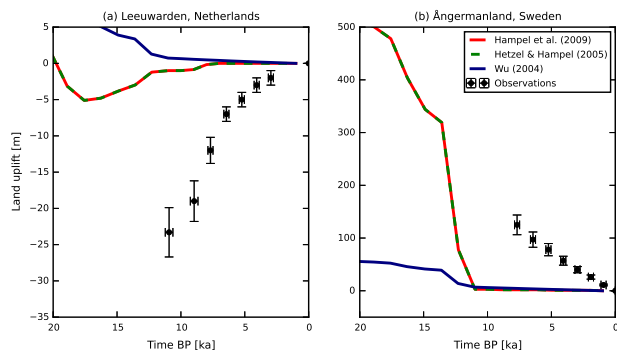


Figure 8.

**Table 1.** Selected results of the models with synthetic ice load. Vertical displacement at the surface and horizontal, vertical and differential stresses at 5 km depth at three locations and four different time points (10 ka - 50% of glaciation, 20 ka - maximum glaciation, 30 ka - end of deglaciation, 40 ka - 10 ka after the end of deglaciation).

	Model HA			Model WU		
	0 km	100 km	500 km	0 km	100 km	500 km
Vertical displacement at 10 ka [m]	-38.6	-31.2	1.0	-21.8	-16.6	1.6
Vertical displacement at 20 ka [m]	-78.1	-62.9	2.1	-52.4	-40.4	4.2
Vertical displacement at 30 ka [m]	-2.5	-1.3	0.4	-19.4	-15.7	1.7
Vertical displacement at 40 ka [m]	-2.4	-1.2	0.3	-4.4	-3.3	-0.7
Horizontal stress at 10 ka [MPa]	-4.0	-2.0	0.5	-3.2	-1.5	0.4
Horizontal stress at 20 ka [MPa]	-8.0	-4.0	1.1	-7.5	-3.7	0.9
Horizontal stress at 30 ka [MPa]	-0.2	0.0	-0.1	-2.1	-1.3	0.3
Horizontal stress at 40 ka [MPa]	-0.2	0.0	-0.1	-0.4	-0.2	-0.1
Vertical stress at 10 ka [MPa]	-2.2	-1.1	0.0	-2.2	-1.1	0.0
Vertical stress at 20 ka [MPa]	-4.4	-2.1	0.0	-4.4	-2.2	0.0
Vertical stress at 30 ka [MPa]	0.0	0.0	0.0	0.0	0.0	0.0
Vertical stress at 40 ka [MPa]	0.0	0.0	0.0	0.0	0.0	0.0
Differential stress at 10 ka [MPa]	1.8	1.5	0.5	1.0	1.1	0.4
Differential stress at 20 ka [MPa]	3.7	2.9	1.1	3.1	2.6	0.9
Differential stress at 30 ka [MPa]	0.2	0.1	0.1	2.1	1.3	0.3
Differential stress at 40 ka [MPa]	0.2	0.1	0.1	0.4	0.2	0.1